Atmospheric and Oceanic Science Letters

ISSN: 1674-2834 (Print) 2376-6123 (Online) Journal homepage: www.tandfonline.com/journals/taos20

Sensitivity of warm-sector heavy precipitation to the impact of anthropogenic heating in South China

LI Shu-Wen, YANG Shuai & LIU Hai-Wen

To cite this article: LI Shu-Wen, YANG Shuai & LIU Hai-Wen (2018) Sensitivity of warm-sector heavy precipitation to the impact of anthropogenic heating in South China, Atmospheric and Oceanic Science Letters, 11:3, 236-245, DOI: 10.1080/16742834.2018.1469952

To link to this article: https://doi.org/10.1080/16742834.2018.1469952

Published online: 14 Jun 2018.

ATMOSPHERIC AND OCEANIC SCIENCE LETTERS
2018, VOL. 11, NO. 3, 236–245
https://doi.org/10.1080/16742834.2018.1469952

Taylor & Francis
Taylor & Francis Group

ARTICLE

Sensitivity of warm-sector heavy precipitation to the impact of anthropogenic heating in South China

LI Shu-Wen[a,b], YANG Shuai[b] and LIU Hai-Wen[a,c]

[a]School of Atmospheric Sciences, Chengdu University of Information Technology, Chengdu, China; [b]Laboratory of Cloud-Precipitation Physics and Severe Storms (LACS), Institute of Atmospheric Physics, Chinese Academy of Sciences, Beijing, China; [c]Department of Aviation Meteorology, Civil Aviation University of China, Tianjin, China

ABSTRACT

Previous studies have mostly focused on the effect of anthropogenic heating (AH) on air pollution events. However, few studies have investigated the impact of AH on the warm-sector precipitation over South China. By using the Weather Research and Forecasting model (WRF) coupled with an urban canopy model with appropriate AH release values, the warm-sector heavy rainfall event that occurred over the Pearl River Delta (PRD) during 8 May 2014 was investigated. The results show that the warm-sector precipitation of the PRD is sensitive to the impact of AH. By affecting the convection in the initiation of precipitation, AH can reduce the total precipitation of urban areas by approximately 10%. The possible mechanism by which AH influences the warm-sector heavy precipitation is described as follows: AH induced local convergence shifts towards the border of the PRD and intensified the convection and precipitation therein, by rearranging the thermal distributions of the flow field. In addition, AH changed the local convergence within the urban PRD areas, which was weakened by the homogenous urban thermal environment, and thereby decreased the total urban precipitation.

摘要

为探讨人为热(AH)对华南暖区暴雨的影响，该文利用WRF-SLUCM模式并考虑适当的AH释放，对2014年5月8日发生在珠江三角洲（PRD）的暖区暴雨进行了数值模拟。有无AH效应的模拟结果分析表明，降水对AH的影响敏感，AH效应使得城区总降水量减少约10%。影响的可能机制为：AH增加导致的热力场和流场再分布，使得局地辐合向PRD边界区域转移增强城乡边界的对流和降水；PRD城区内更为均质的城市热环境减小了热力对比削弱了辐合，从而降低了城区降水。

ARTICLE HISTORY
Received 22 September 2017
Revised 8 January 2018
Accepted 31 January 2018

KEYWORDS
Heavy precipitation; anthropogenic heating; numerical simulation

关键字
暴雨; 人为热; 数值模拟

1 Introduction

In recent decades, the Pearl River Delta (PRD) has experienced rapid urbanization and economic development, characterized by land use changes and the explosive growth of both population and overloaded energy expenditures. In addition, the extent of anthropogenic heating (AH) is synchronously increasing due to the excessive releases of waste heat from vehicles, air-conditioning systems, factories, and even human bodies during the process of physiological metabolism (Allen, Lindberg, and Grimmond 2011; Sugawara and Narita 2008). As an important component of the near-ground energy balance equation (Sailor 2011), AH influences local heat fluxes and changes local circulation, aggravating the urban heat island effect (Ichinose, Shimodozono, and Hanaki 1999). This kind of effect might transfer upwards and spread to the atmospheric planetary boundary layer or even the higher troposphere, thus impacting the thermal or dynamical structure of these areas (Yu et al. 2014). These direct and indirect effects of AH have caused a series of problems in environmental, climatological, and synoptic realms (Feng et al. 2012; Narumi, Kondo, and Shimoda 2009; Nie et al. 2017; Yu et al. 2014).

There are quite a few studies on the impact of the urbanization effect on synoptic-scale processes, including precipitation (Chen, Yang, and Wu 2016; Feng et al. 2012; Miao et al. 2011; Yang et al. 2014). However, as an important heat source, the AH effect on warm-sector precipitation has been rarely studied. Although urbanization is important for the release of AH, the magnitude of AH does not have the absolutely linear dependance on urban size. To determine the urbanization effect, it is necessary to further quantify the impact of AH as an independent factor on the precipitation of the Pearl River Delta (PRD), especially for thermally dominant, warm-sector precipitation.

AH could influence the thermodynamic structure of urban areas by changing the near-ground temperature

CONTACT YANG Shuai yangs@mail.iap.ac.cn

(Ichinose, Shimodozono, and Hanaki 1999; Narumi, Kondo, and Shimoda 2009). By enhancing the upwards heat flux, it modifies the height of the free convection level, lifted condensation level, and planetary boundary layer (PBL). These effects indirectly change the rainfall amount and intensity over urban areas (Nie et al. 2017; Yang et al. 2014). Chen, Yang, and Wu (2016) found that the combined impacts of urbanization and AH increased the precipitation in Hangzhou city by 1.2% in the winter and 14.4% in the summer by the enhancement of low-level convergence, while Feng et al. (2012) reported a noteworthy decrease in the precipitation of the Yangtze River Delta region.

The PRD is in South China, adjacent to the South China Sea and Western Pacific Ocean, and it experiences warm-sector heavy precipitation in the summer. Due to a lack of evident weather systems and strong local characteristics, it is particularly difficult to perform perfect simulations and predict the warm-sector heavy rainfall in the PRD (He, Chen, and Kong 2016). To improve simulation efforts, local thermal factors such as urbanization and the AH effect should be sufficiently considered, especially for this type of thermally dominant precipitation. However, first, the sensitivity of the warm-sector heavy precipitation in South China to the impacts of AH needs testing. Therefore, the aims of this study are as follows: 1) to determine whether the simulation of warm-sector heavy precipitation in South China is sensitive to imposed AH releases with an urban canopy model implanted in a WRF model; 2) if so, based on both the locations and amounts of precipitation, determine how to quantify this kind of change due to AH; and 3) address the possible mechanisms by which the AH releases change the warm-sector heavy precipitation of South China. To address these goals, this study has been arranged as follows: in section 2, the models, data, and experimental design will be introduced. By invoking high-resolution simulations, and performing sensitive experiments, the influence of AH will be explored as an independent factor with the warm-sector precipitation case in section 3. A summary of the study will be given in the last section.

2 Models, data, and experimental design

2.1 *Models and data*

The Weather Research and Forecasting (WRF, V3.6.1) model, coupled with a sophisticated single-layer urban canopy model (SLUCM), was utilized to study the response of the warm-sector precipitation to the AH release (AHR) (Chen et al. 2011). With the SLUCM, the AH and its diurnal variation were considered by adding them to the sensible heat flux from the urban canopy layer. A two-way nested model was implemented for two domains (Figure 1(a)), with horizontal grid points of 350 × 350 and 448 × 340 and spatial resolutions of 9 and 3 km, respectively. The main physical parameters included the WRF Double Moment 5-class graupel microphysics scheme and the BouLac PBL planetary boundary layer scheme. The outer domain employed the Betts-Miller-Janjic cumulus scheme. The model integration lasted 36 hours, spanning from 1800 UTC 7 to 0000 UTC 9 May 2014.

The six-hour 1° × 1° Global Final (FNL) reanalysis data of the National Centers for Environmental Prediction (NCEP) was employed to the WRF model. In addition, we used the updated Moderate Resolution Imaging

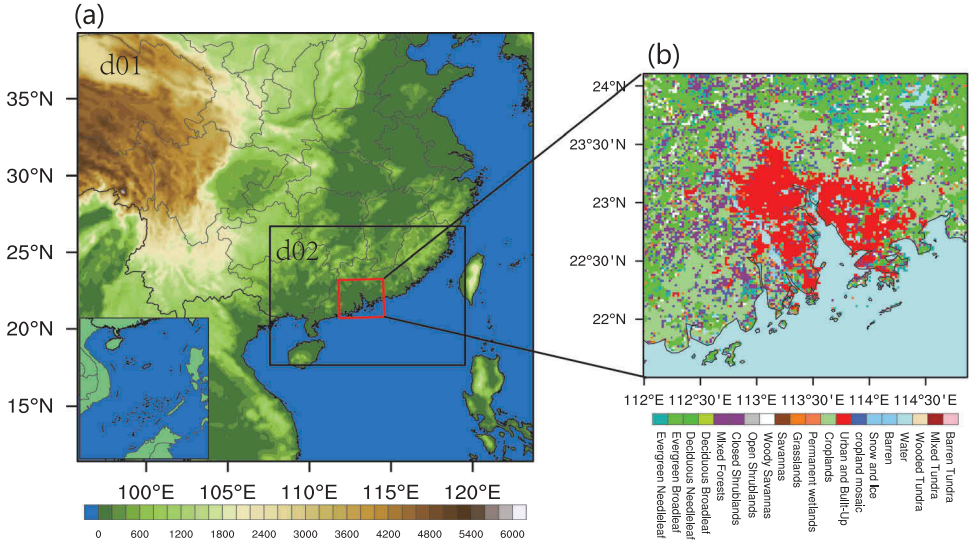

Figure 1. (a) WRF domain configuration and location at the PRD (red rectangle). (b) Land use map for the PRD region in the WRF.

Spectroradiometer (MODIS) 20-category land use/land cover data (Xie et al. 2016) to perform the simulation as a control experiment without the AH. Figure 1(b) shows the map of the different land use categories in the PRD region, where the red parts represent the urban coverage. In this study, the hourly precipitation products from automatic meteorological stations in China (http://cdc.cma.gov.cn/) were used as observations to validate the simulation.

2.2 *Description of the numerical experiments*

The AH release, which should not be ignored (Chen, Yang, and Wu 2016), is seldom taken into consideration as an independent factor, especially for simulating the thermally dominant warm-sector precipitation in the PRD. A lack of an accurate and universally standardized lists of AH emissions may be the main reason for this problem.

To address these restrictions, the AH flux in Guangzhou, which had a maximal value of approximately 50 $W{\cdot}m^{-2}$ and was recently estimated by Zhu et al. (2017), was utilized as an example to illustrate the quantitative influence of AH on precipitation. Based on the AHR peak (Zhu et al., 2017), a fixed (constant) diurnal AH profile was derived as a benchmark (denoted as 1.0AH in the experiment below). Then, various attempts at simulating the effects of AH were performed with the SLUCM option. Thus, the pure AHR represented an independent factor influencing precipitation, exclusive of the other urbanization effects. First, the AHR was turned off during the control experiment (0.0AH). Second, the AHR option was turned on during sensitive experiments with different AH values, which were named the 1.0AH- (i.e. 1.0 times of AH benchmark value, the same below), 1.5AH-, and 2.0AH-experiments. By comparatively analyzing the differences among these experiments, the problems described in the introduction were solved.

3 Results

3.1 *General description of the precipitation case*

From 0000 UTC 8 to 0000 UTC 9 May 2014, heavy rainfall occurred around the PRD region of South China, leading to city waterlogging. It was classified as warm-sector precipitation by the National Meteorological Center. That type of local heavy rainfall event has been common in the PRD during the summer months of recent years, which has become a great threat to the local residents of high-density urban areas.

Figure 2 gives the synoptic charts for the four representative times before and during the precipitation event by using the 1° × 1° NCEP/NCAR data. The temporal evolutions of the geopotential height at 500 hPa, together with the wind speed and relative humidity at 850 hPa, are delineated. Before the precipitation began (Figure 2(a)), the PRD region (outlined by the red frame) was dominated by wide southwesterly from the ocean, which brought a large amount of warm, moist airflows. No large trough or ridge was present above the PRD. Until 0600 UTC (Figure 2(b)), a weak upper-level trough (red curved line) presented in the western PRD, and then it moved over the gulf and the eastern PRD at 1200 UTC (Figure 2(c)), and shifted out of the frame (Figure 2(d)). Albeit a weaker trough, it sped up the low-level southwesterly and accelerated the transport of the warm, moist airflow, which was particularly evident at the time when the precipitation intensified (Figure 2(b) and (c), as well as Figure 3). Therefore, the above analyses indicate that the large-scale quasigeostrophic situations did not provide favorable conditions for convection organization, since there was a homogeneous southwesterly and no deployment of a large-scale weather system development (Figure 2(a)). However, the approaching regional-scale weak trough with a comparable size to the precipitation system was superposed above the enhanced southwesterly, which appears to have encouraged the development of precipitation.

3.2 *Model evaluations*

Since the primary concern of this study was the impact of AH on precipitation, the simulated precipitation without AH (i.e. the 0.0AH experiment shown in Figure 3(a), shaded) and with AH (i.e. the 1.0AH experiment, Figure 3(b)) were compared against observations from the hourly encrypted automatic station (shaded circle). The overall precipitation period from 0000 UTC 8 to 0000 UTC 9 May experienced a process similar to the one previously described; it was initialized in the west of the PRD region, after which it moved across the bay, arrived at the eastern part of the PRD, and finally dissipated. There were two precipitation centers. One was located west of the PRD, centered at (22.4°N, 112.5°E) (see green frame shown in Figure 3(b)), and the other was surrounding the city clusters of the PRD (red frame, Figure 3(b)). For the control experiment without AH (0.0AH experiment, Figure 3(a)), the simulated left-branch rain belt west of 113.25°E (green box) was north of its observed location, while the precipitation intensity of the right-branch rain belt (red box) was a little overestimated relative to the observed value (cf. the difference of the color scale). The simulations that considered the effects of AH (i.e. the 1.0AH experiment,

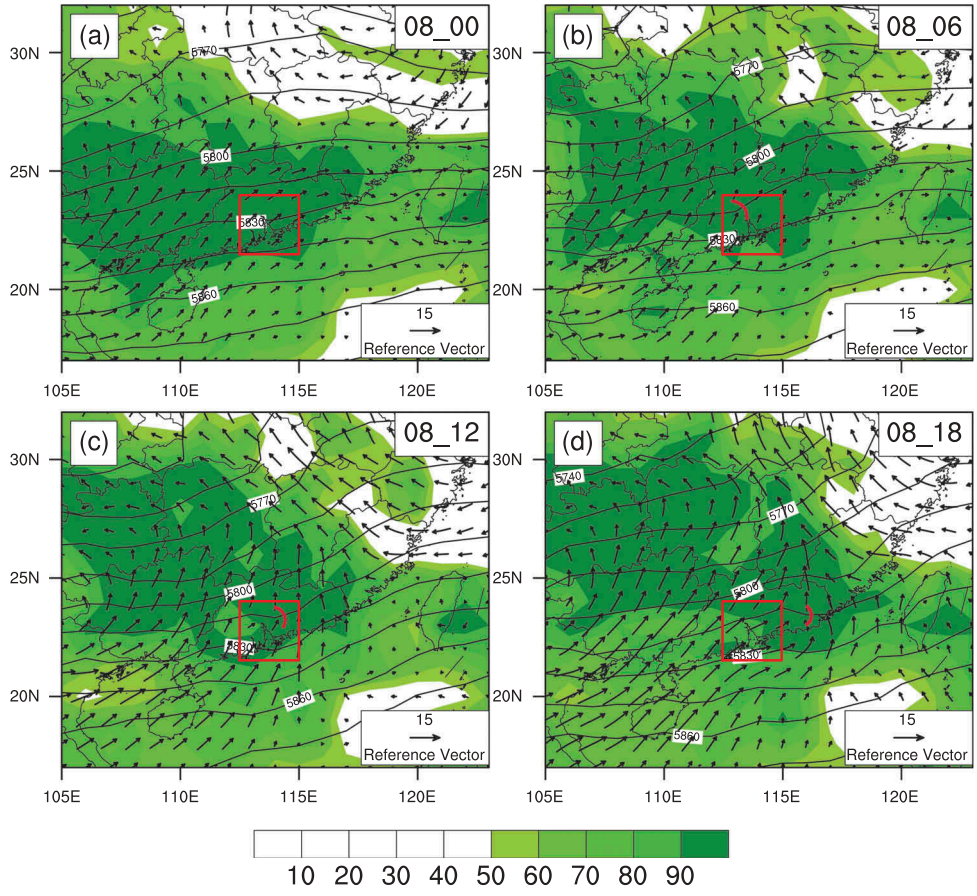

Figure 2. Synoptic charts of wind vector (m s^{-1}) and relative humidity (shaded, %) at the 850 hPa level and the geopotential height at the 500 hPa level (isolines, dgpm) at (a) 0000 UTC, (b) 0600 UTC, (c) 1200 UTC, and (d) 1800 UTC on 8 May 2014. The weak shortwave trough is denoted by red curves in (b)–(d).

Figure 3(b)), performed better than the 0.0AH experiment simulation. For example, the left-branch precipitation moved southwards and gradually approached its observed location, and the right-branch precipitation intensity and coverage decreased, reaching levels that were closer to the observed values than those of the control test. Furthermore, the precipitation location was more concentrated near the PRD. Although the station-observed precipitation in excess of 100 mm (west of 112.5°E) was not reproduced well in the 1.0AH experiment, we paid more attention to the PRD urban region and its surrounding areas in this study, since the AH releases are mainly concentrated at urban regions.

In short, by considering the AH, the simulation of both the location and amount of precipitation were refreshed, at least for this case. Based on these results, we posited another question: if the AHR continues increasing, will the simulation performance improve? To investigate this question, and additional two experiments, 1.5AH and 2.0AH, are supplemented. However, these additional simulations did not yield the expected good results. The precipitation of the 1.5AH simulation shifted towards the downwind areas of the PRD. The 2.0AH simulation delineated scattered precipitation locations, dispersing to the west of the PRD region. Based on the results of these contrasting experiments, when the appropriate AHR is injected into the model, it might improve the precipitation simulations, but this ameliorated effect cannot be infinitely amplified. It seems that only the consideration of a practical AHR is advantageous in numerical simulations.

3.3 *Results contrasts among diverse experiments and possible mechanism responsible for the differences*

To quantify the influence of AH on precipitation, the regional-precipitation evolutions of both urban (red box) and nearby rural (green box) areas were compared during the entire simulation period (Figure 3(e) and (f)). The precipitation started at 00 00 UTC 8 May 2014 and increased up to 20 mm within six hours for both the

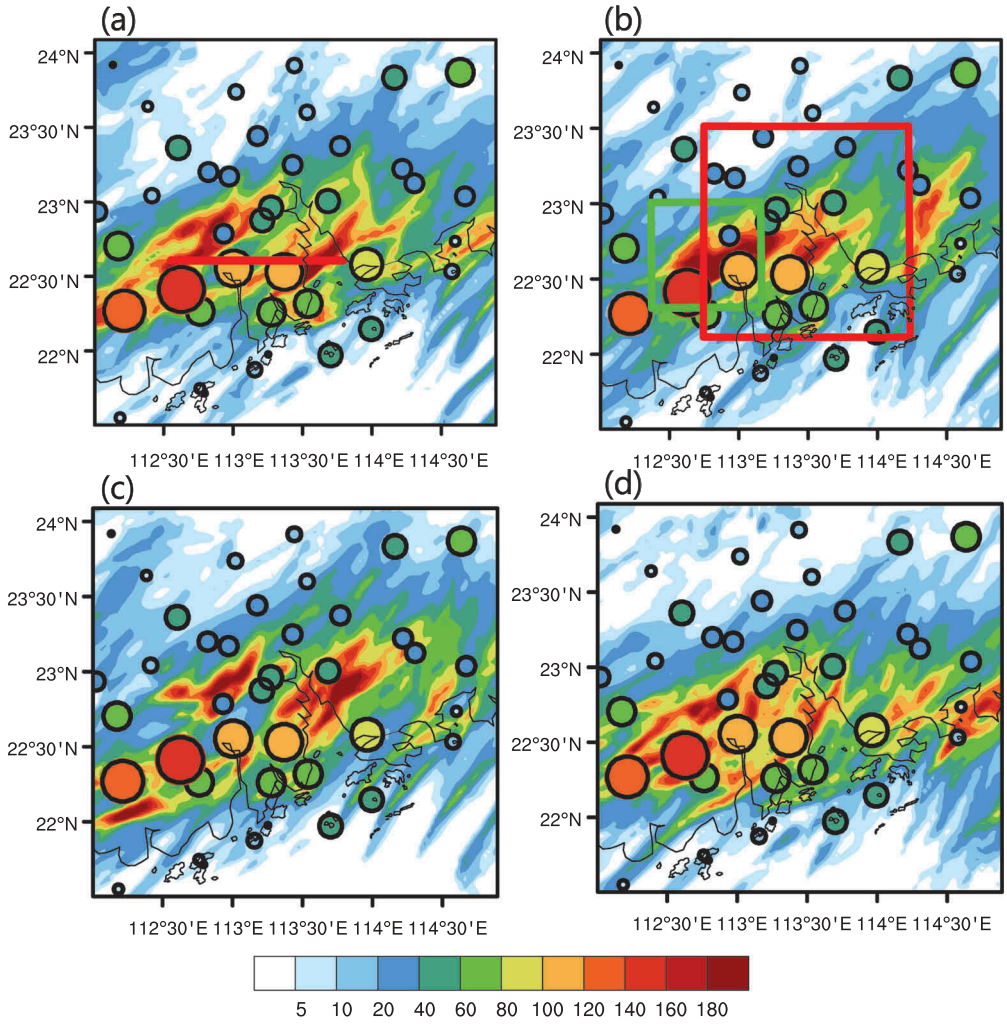

Figure 3. Simulated and observed precipitation (shaded, mm) from 1200 UTC to 2100 UTC 8 May for (a) 0.0AH, (b) 1.0AH, (c) 1.5AH and (d) 2.0AH experiments. The intensive observations by meteorological stations are depicted by shaded circles, with sizes proportional to the precipitation amount (cf., the commonly used color scale). The red solid line in (a) denotes the location of the vertical cross sections used in Figure 4(d1) and (d2). The subdomains enclosed by the red and green rectangles in (b) are used to calculate the PRD urban and nearby rural precipitation in Figure 3(e) and (f), respectively. The evolution of the accumulative precipitation (mm) in (e) the PRD urban regions (within the red frame in Figure 3(b) and (f) nearby rural areas (green box in Figure 3 (b)) is shown for different simulations from 1800 UTC 7 to 0000 UTC 9 May 2014. The diurnal profiles of (g) the sensible heat flux (W m^{-2}) and (h) the planetary boundary layer height in meters are shown for the same period as (e) and (f).

urban and rural areas. From 0800 UTC, the rural precipitation swiftly increased to its peak value (above 120 mm for four simulations, with a maximal value of approximately 150 mm) at 1700 UTC. Then, it tended to gently evolve, which means that the precipitation passed through the territory of the target region. In contrast, the urban precipitation passed through a buffer zone before it rapidly increased at 13 00UTC and reached a peak point (below 120 mm, less than the rural peak value) at 19 UTC, two hours later than the rural precipitation. This is coincident with the west-to-east propagation of the precipitation and consistent with the stronger precipitation of the left-branch than the right-branch, as shown in Figure 3(b).

More specific differences in the precipitation were distinguished among the four simulations. Relative to the control experiment (blue line), the accumulative precipitation in the urban regions of the PRD (Figure 3 (e)) for the 1.0AH experiment (yellow line) obviously and consistently decreased, with a maximal deficit of approximately 10 mm, accounting for 10% of the regionally averaged total precipitation. However, the average rural precipitation difference between the 0.0AH and 1.0AH experiments had a completely out-of-phase tendency (of consistent growth with a maximum value of approximately 20 mm), increasing by 13% of the total rural precipitation amount (Figure 3 (f)). This occurred because of the shift of the major

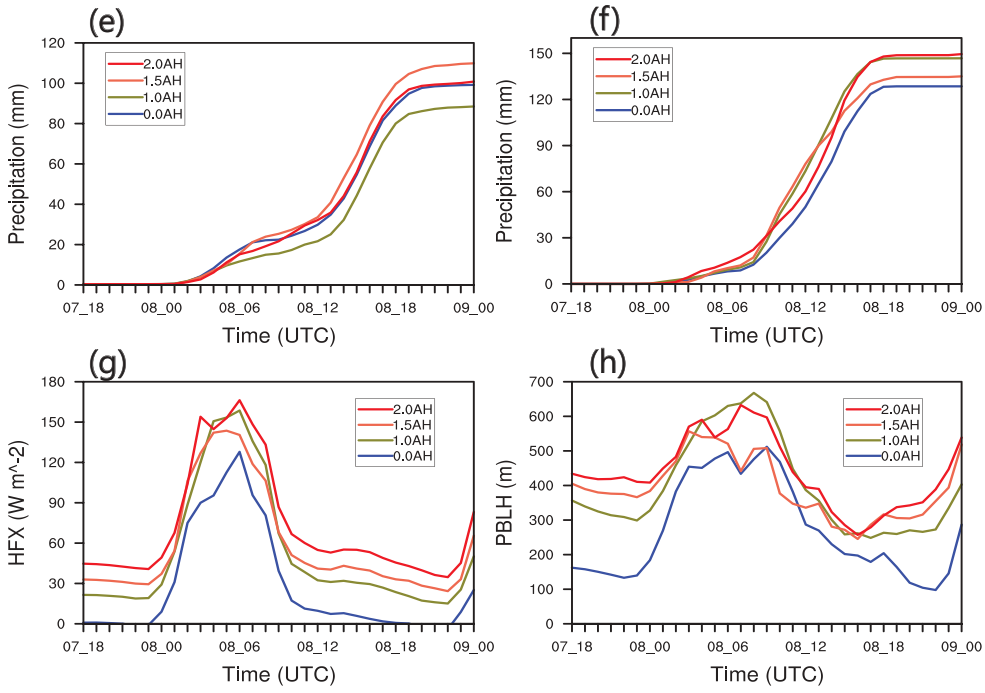

Figure 3. (Continued).

precipitation center, which advanced to a location at the western ambient areas of the PRD (Figure 3(a) and b)). Including the other two experiments, the precipitation differences of the four simulations were not apparent at the beginning of the simulation (before 0800 UTC in the rural area and before 1200 UTC in urban area). The greatest differences among the experiments occurred during intensive precipitation stages. Particularly after 1200 UTC, the urban precipitation (Figure 3(e)) experienced an increase from the 1.0AH to the 1.5AH experiment. Then, the urban precipitation for the 2.0AH experiment fell back to the value of the control (0.0AH) experiment. The comparison revealed that the optimal AHR (1.0AH) decreased the urban precipitation relative to the control experiment because of its shift to the ambient rural areas. While overestimating the AH by keeping the growth factor (from 1.0AH/1.5AH to 1.5AH/2.0AH for the case of this study) might, to a certain extent, cause the intensification or reduction of the precipitation in the urban region. Ultimately, unreasonable values may be derived by the overestimation.

Figure 3(g) and (h) show the sensitivity of the sensible heat flux (HFX) and PBL height in urban regions to the gradual growth of the AH above the urban underlying surface. In general, all the temporal profiles of the HFX (Figure 3(g)) had similar diurnal tendencies, with midday (0600 UTC) peaks due to the solar radiation. The PBL heights (Figure 3(h)) represent a diurnal evolution that is nearly synchronous with that of the HFXs, except that two PBL peaks coexist, with the larger peaks later than those of HFXs. Basically, the PBL height increased with increasing HFX. The excessive heat flux directly strengthened water vapor mixing in the PBL and increased the PBL height over the urban region, translating to higher PBL altitudes (Yang et al. 2014).

In principle, increased AH results in increased values of the HFX, because AH and its diurnal variation are added to the sensible heat flux from the urban canopy layer (Chen et al. 2011). In this case, both the HFX value and the PBL height coincidently increased with increasing AH before precipitation occurred (at 0000 UTC 8 herein). Once the precipitation began, the situation changed. Until 1000 UTC and 1800 UTC 8, the HFX value and PBL height sequentially returned to their original levels. The feedback of the precipitation changed the regular impact of the AH on the thermal and dynamical structure of the atmospheric boundary layer, which made the case complex. Generally, the 0.0AH experiment produced the smallest HFX value and lowest PBL height, relative to the three experiments that incorporated AH into the simulation. This is very clearly shown during the entire simulation period, except for the PBL height between 0900 UTC and 11 UTC 8 shown in Figure 3(h).

To explore the controlling mechanism of how AH affects precipitation, an extended analysis on the meteorological factors that are closely related to precipitation was conducted. Figure 4(a1) illuminates the 2-m temperature (T_2) and the 10-m wind vector (U_{10}) in

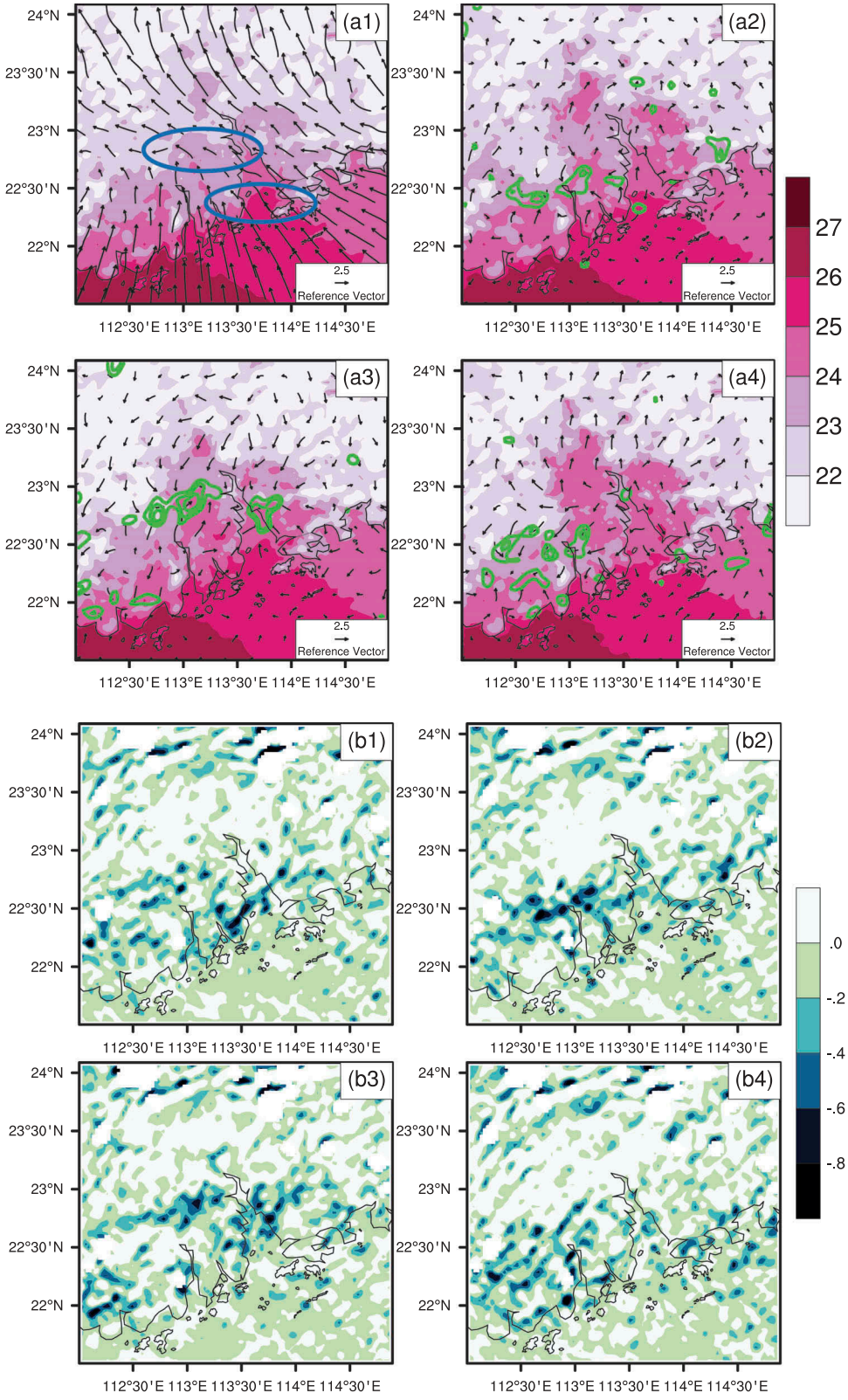

Figure 4. (a) The distributions of (a1) 2 m temperature (T_2, shaded, °C) and 10 m wind vector (U_{10}) averaged from 1200 UTC to 1800 UTC 8 May for the control experiment. The averaged T_2 and the differences of U_{10} between the sensitive experiments and control simulation are shown in (a2) for 1.0AH-0.0AH, (a3) for 1.5AH-0.0AH, and (a4) for 2.0AH-0.0AH. The changes in the convergence field (thick green line, 10^{-4} s^{-1}) relative to the control experiment is also superposed. (b1–b4) shows the averaged convergence field (10^{-3} s^{-1}) and (c1–c4) shows the specific humidity (g/kg) for the four simulations at the 750 hPa level for the same period. (d1) and (d2) are the cross sections (along the red line in Figure 3(a)) of upward motion (shaded, m s^{-1}), superposed with the in-plane flow vector (m s^{-1}, where the vertical velocity is enlarged tenfold) during the period of 12 UTC–18 UTC 8 May 2014.

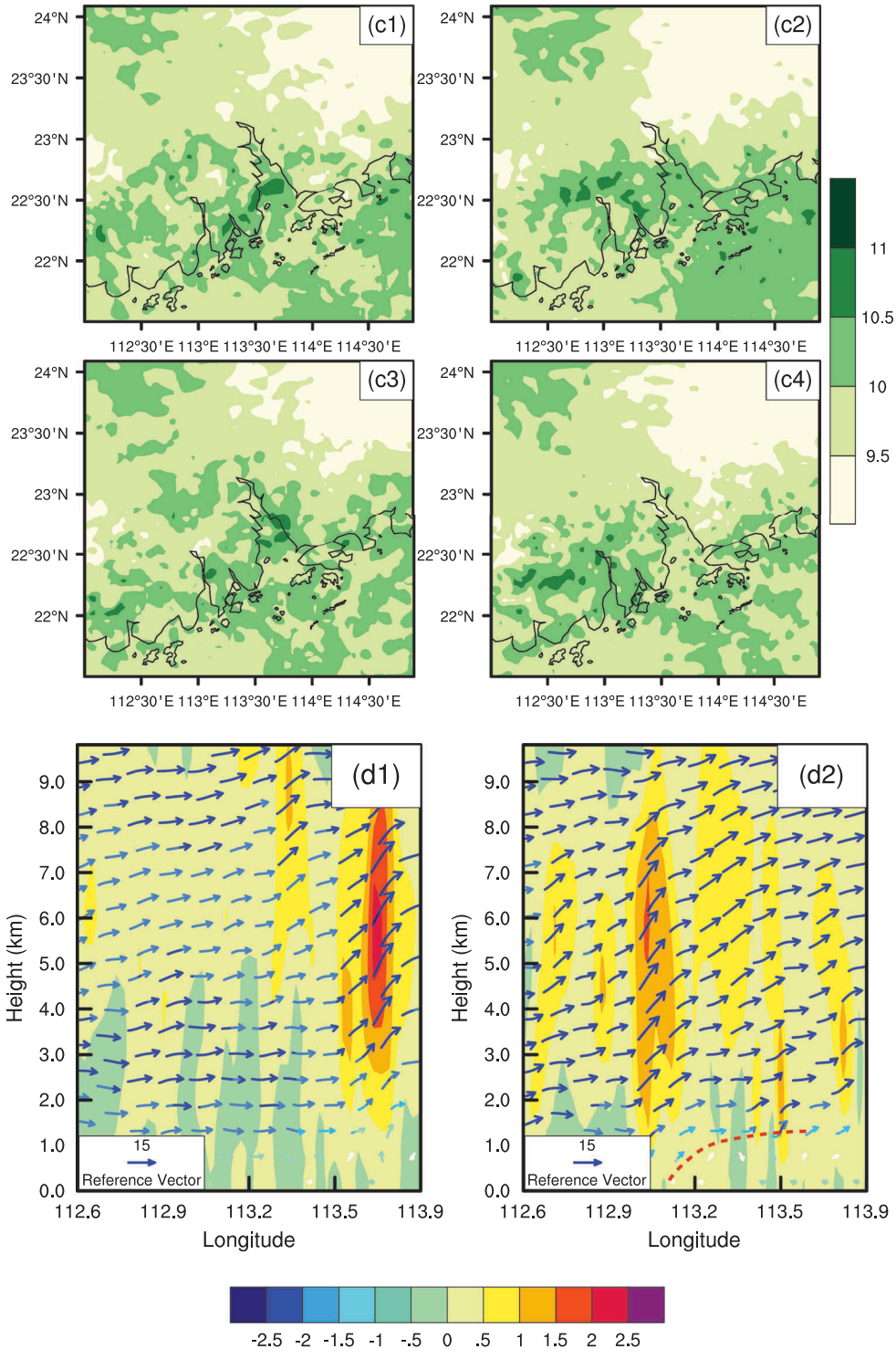

Figure 4. (Continued).

the control experiment averaged from 1200 UTC to 1800 UTC on 8 May. Figure 4(a2)–(a4) depicts the T_2 of the three AH-sensitive experiments and the U_{10} difference between the AH-sensitive experiments and the control. For the control experiment, the method by which the two rain cells (shown in Figure 3(a)) were triggered could be clearly resolved using the images of the fine-scale simulation. West of 113.25°E, the wind direction shear near 23°N (see left blue circle, Figure 4(a) led to the initiation of the local convergence and convection related to the left-branch precipitation. The right-branch precipitation in the PRD might be initiated by obvious land-sea thermal differences and wind-speed convergences (right blue circle,

Figure 4(a1). For the different precipitation patterns observed in experiments that considered the effects of AH, the initiation of the rain cells was mainly determined by the change in location of the convergence (green thick line). For example, the sporadic convergence in Figure 4(a4) corresponded to the scattered distribution of the precipitation cells (cf. Figure 3(d)). The 1.0AH experiment shown in Figure 4(a2) should be described in more detail because it yielded the optimal simulation in this study. Experiment 1.0AH showed that AH played a role in outlining a clearer urban area boundary that reflects the boundaries depicted by the land use map in Figure 1(b). This also reduced the thermal contrast within the PRD urban areas, decreasing the local vertical convection (cf. near 113.65°E at the vertical-cross sections in Figure 4(d2)). It led to weakened urban precipitation based on both the precipitation coverage and intensity (Figure 3(a) and(b)). The flow field changed as the thermal distributions reshuffled, which induced a shift in the convergence boundary towards the areas surrounding the PRD with larger thermal gradients.

Figure 4(b1)–(b4) and (c1)–(c4) illustrate the distributions of the near-surface convergence pattern and lower troposphere specific humidity. Ziegler and Rasmussen (1998) reported that the depth and intensity of the convergence and updrafts, rather than the surface convergence alone, played a pivotal role in the initiation of deep convection. Therefore, in addition to the 10 m wind vector shown in Figure 4(a1)-(a4), the low troposphere convergence is emphasized again in Figure 4(b1)-(b4). This figure demonstrates that the local convergences and their changes for several experiments match the locations of precipitation and corresponding shifts. For example, a strong convergence belt in the center of the PRD region for the control experiment was weakened and transferred to the western PRD in the 1.0AH experiment, moved downwind to the northern PRD in the 1.5AH experiment and became more scattered along the coastline in the 2.0AH experiment. Combined with the 10 m wind convergence data, this illustrates that the propagation of precipitation basically synchronizes with the overall course of variations in the convergence. Because of the continuous and plentiful moisture supply by the southwesterly from the neighboring South China Sea, the changes in the moisture patterns of the diverse experiments (Figure 4(c1)-(c4)) depended mostly on various local convergences (Figure 4(a1)-(a4) and 4 (b1)-(b4)).

For the control experiment (0.0AH) and optimal simulation (1.0AH) described above, the vertical cross section of the vertical velocity and circulation is given in Figure 4 (d1) and (d2). In Figure 4(d1), the strong updrafts above 113.65°E correspond well to the PRD precipitation center in Figure 3a for the control experiment. However, the vertically ascending motion therein was obviously weakened in the optimal simulation with AH (Figure 4(d2)), although a hot plume (red dashed curve) presenting between 113.01–113.65°E below 1.5 km occurred due to the increasing upward heat flux by AH. Above 113.01°E, an updraft branch developed at the border of the reconstructed highly thermal environment field within the PRD. The hindering of the hot plume and the border effect with a large thermal contrast led to the new convection that developed above 113.01°E. Correspondingly, the precipitation shifted towards this area (Figure 3(a) and (b)). The upstream dry down effect, together with the weakening of the local convergence due to the homogenous urban thermal environment, decreased precipitation in the PRD urban areas (Figure 3(b)).

4 Summary

In this study, a numerical simulation was performed for a thermally dominant warm-sector rainstorm event by utilizing a coupled WRF-SLUCM model. Based on the sensitive experiments with various AH profiles, the responses of precipitation on AH were investigated. The main conclusions are summarized as follows.

(1) For the warm-sector precipitation process in South China, the environmental conditions and initiation factors were demonstrated. The homogeneous southwesterly prevailed over the PRD region. No distinct large-scale weather systems developed. This indicates that large-scale situations do not provide favorable conditions for convection organization. By invoking a high-resolution simulation, the wind direction shear and wind speed convergence overlapped and created obvious thermal contrast, co-acting to lead to the local convergence and convection related to the initiation of the precipitation.

(2) The impact of AH was further analyzed by several sensitive experiments. They showed that the simulation performance in simulating both the location and amount of the precipitation are optimal when the case-appropriate AH value is used. Note that two additional experiments with a continuous injection of AH did not reveal that the precipitation simulation performance indefinitely increases with increasing AH. Seemingly, overly high AHRs might have a negative effect on the simulation performance. When only practical AHRs are considered, AH has its optimal effect in numerical simulations.

(3) For simulations that considered AH, differences in the precipitation patterns were mainly determined by the location change of the convergent boundary. The flow field changed as the thermal distributions were rearranged due to the AH, which induced local convergence shifts towards the border of the PRD and intensified the convection and precipitation therein. The dry-down effect due to upstream rain, together with the weakening of the local convergence because of the homogenous urban thermal environment, decreased the precipitation in the PRD urban areas.

Acknowledgments

The authors are supported by the Special Scientific Research Fund of the Meteorological Public Welfare of the Ministry of Sciences and Technology, China (Grant No. GYHY201406003), the National Natural Science Foundation of China (Grant Nos. 41375054, 41575064, and 41375052), the Applied Basic Research Programs of the Science and Technology Department of Sichuan Province (Grant No. 2015JY0109), and the Starting Foundation of Civil Aviation University of China (Grant No. 2016QD05X).

Disclosure statement

No potential conflict of interest was reported by the authors.

References

Allen, L., F. Lindberg, and C. S. B. Grimmond. 2011. "Global to City Scale Urban Anthropogenic Heat Flux: Model and Variability." *International Journal of Climatology* 31 (13): 1990–2005. doi:10.1002/joc.2210.

Chen, F., H. Kusaka, R. Bornstein, J. Ching, C. S. B. Grimmond, S. Grossman-Clarke, T. Loridan, et al. 2011. "The Integrated WRF/Urban Modelling System: Development, Evaluation, and Applications to Urban Environmental Problems." *International Journal of Climatology* 31 (2): 273–288. doi:10.1002/joc.2158.

Chen, F., X. Yang, and J. Wu. 2016. "Simulation of the Urban Climate in a Chinese Megacity with Spatially Heterogeneous Anthropogenic Heat Data." *Journal of Geophysical Research: Atmospheres* 121 (10): 5193–5212.

Feng, J. M., Y. L. Wang, Z. G. Ma, and Y. H. Liu. 2012. "Simulating the Regional Impacts of Urbanization and Anthropogenic Heat Release on Climate across China." *Journal of Climate* 25 (20): 7187–7203. doi:10.1175/JCLI-D-11-00333.1.

He, L., T. Chen, and Q. Kong. 2016. "Research Progress of Heavy Rainfall in South China Warm Region." [In Chinese.] *Journal of Applied Meteorological Science* 27 (05): 559–569.

Ichinose, T., K. Shimodozono, and K. Hanaki. 1999. "Impact of Anthropogenic Heat on Urban Climate in Tokyo." *Atmospheric Environment* 33 (24–25): 3897–3909. doi:10.1016/S1352-2310(99)00132-6.

Miao, S., F. Chen, Q. Li, and S. Fan. 2011. "Impacts of Urban Processes and Urbanization on Summer Precipitation: A Case Study of Heavy Rainfall in Beijing on 1 August 2006." *Journal of Applied Meteorology and Climatology* 50 (4): 806–825. doi:10.1175/2010JAMC2513.1.

Narumi, D., A. Kondo, and Y. Shimoda. 2009. "Effects of Anthropogenic Heat Release upon the Urban Climate in a Japanese Megacity." *Environ Res* 109 (4): 421–431. doi:10.1016/j.envres.2009.02.013.

Nie, W., B. F. Zaitchik, G. Ni, and T. Sun. 2017. "Impacts of Anthropogenic Heat on Summertime Rainfall in Beijing." *Journal of Hydrometeorology* 18 (3): 693–712. doi:10.1175/JHM-D-16-0173.1.

Sailor, D. J. 2011. "A Review of Methods for Estimating Anthropogenic Heat and Moisture Emissions in the Urban Environment." *International Journal of Climatology* 31 (2): 189–199. doi:10.1002/joc.v31.2.

Sugawara, H., and K. I. Narita. 2008. "Roughness Length for Heat over an Urban Canopy." *Theoretical and Applied Climatology* 95 (3–4): 291–299. doi:10.1007/s00704-008-0007-7.

Xie, M., J. Liao, T. Wang, K. Zhu, B. Zhuang, Y. Han, M. Li, and S. Li. 2016. "Modeling of the Anthropogenic Heat Flux and Its Effect on Regional Meteorology and Air Quality over the Yangtze River Delta Region, China." *Atmospheric Chemistry & Physics Discussions* 15 (22): 32367–32412. doi:10.5194/acpd-15-32367-2015.

Yang, L., F. Tian, J. A. Smith, and H. Hu. 2014. "Urban Signatures in the Spatial Clustering of Summer Heavy Rainfall Events over the Beijing Metropolitan Region." *Journal of Geophysical Research: Atmospheres* 119 (3): 1203–1217.

Yu, M., G. R. Carmichael, T. Zhu, and Y. Cheng. 2014. "Sensitivity of Predicted Pollutant Levels to Anthropogenic Heat Emissions in Beijing." *Atmospheric Environment* 89 (2): 169–178. doi:10.1016/j.atmosenv.2014.01.034.

Zhu, K., W. Zhao, M. Xie, X. Zhu, M. Li, and W. Feng. 2017. ""Characteristics of Human Thermal Emission in South China."." [In Chinese.] *Journal of Ecology and Rural Environment* 33 (3): 201–206.

Ziegler, C. L., and E. N. Rasmussen. 1998. ""The Initiation of Moist Convection at the Dryline: Forecasting Issues from a Case Study Perspective."." *Weather and Forecasting* 13 (4): 1106–1131. doi:10.1175/1520-0434(1998)013<1106:TIOMCA>2.0.CO;2.